

Boosting terahertz generation in laser-field ionized gases using a sawtooth wave shape

P. González de Alaiza Martínez,¹ I. Babushkin,² L. Bergé,¹ S. Skupin,³ E. Cabrera-Granado,⁴ C. Köhler,⁵ U. Morgner,² A. Husakou,⁶ and J. Herrmann⁶

¹CEA-DAM, DIF, F-91297 Arpajon, France

²Institute of Quantum Optics, Leibniz University Hannover, Welfengarten 1 30167, Hannover, Germany

³Univ. de Bordeaux - CNRS - CEA, Centre Lasers Intenses et Applications, UMR 5107, 33405 Talence, France

⁴Facultad de Óptica y Optometría, Universidad Complutense de Madrid, 28037, Madrid, Spain

⁵Institute for Scientific Computing, TU Dresden, 01062 Dresden, Germany

⁶Max-Born-Institut für Nichtlineare Optik und Kurzzeitspektroskopie, 12489 Berlin, Germany

(Dated: November 5, 2018)

Broadband ultrashort terahertz (THz) pulses can be produced using plasma generation in a noble gas ionized by femtosecond two-color pulses. Here we demonstrate that, by using multiple-frequency laser pulses, one can obtain a waveform which optimizes the free electron trajectories in such a way that they reach the highest velocity at the electric field extrema. This allows to increase the THz conversion efficiency to the percent level, an unprecedented performance for THz generation in gases. Besides the analytical study of THz generation using a local current model, we perform comprehensive 3D simulations accounting for propagation effects which confirm this prediction. Our results show that THz conversion via tunnel ionization can be greatly improved with well-designed multicolor pulses.

PACS numbers: 42.65.Re, 32.80.Fb, 52.50.Jm

Ultrashort pulses in the terahertz (THz) range (from ~ 0.1 to ~ 30 THz) are extremely important for various time-resolved studies in molecular physics, chemistry, material sciences, and security applications [1–8]. The THz frequency interval lies in between the accessible range of electronic (microwave) and optical (infrared) technologies, often referred to as the THz gap. To access this spectral range, recent investigations proposed to use nonlinear processes in gases ionized by fs laser pulses, which provides higher breakdown thresholds, broader spectral ranges and better tunability in the THz and mid-infrared (MIR) ranges. Field strengths of THz pulses generated by two-color optical pulses are typically limited to the range below 1 MV/cm or pulse energies below 100 nJ [9–15]. The highest THz energy of 5 μJ was obtained in [13] with conversion efficiency of 10^{-4} . The physics behind this so-called photocurrent mechanism can be understood by the peculiarities of tunnel ionization and subsequent dynamics of free electrons in the field [12, 13, 16–19]. It was shown [16, 17, 19] that laser-driven THz emission is related to interactions over two different time scales: the attosecond sub-cycle dynamics of tunnel ionization and the femtosecond pump pulse dynamics. Free electrons, extracted from atoms by ionization in sharp attosecond-long steps [17, 20, 21], are accelerated in the laser field and create a net macroscopic current that contains low frequency components. This current is responsible for the observed THz emission.

In Refs. [16, 17, 19] the spectral shape and energy of the THz pulses generated by the above mechanism have been explained by analogy with linear diffraction theory, where ionization events play the role of slits in a “temporal diffraction grating”. The THz radiation then appears as a zero-diffraction order peak in the corresponding diffrac-

tive pattern. Its amplitude is impacted by each ionization event and is determined not only by the pump field near the ionization instants, but also by the whole pump waveform. This non-instantaneous dependence suggests that, by optimizing the pump field shape, one may achieve higher THz yields for a given pulse energy.

In this article, we exploit degrees of freedom given by appropriately chosen pump waveforms to increase the THz conversion efficiency. We show that the fields with a sawtooth-like temporal shape do promote the highest THz signals triggered by tunnel-induced photocurrents. We predict, by means of a local theory, that sawtooth waveforms can in principle increase the THz efficiency by up to two orders of magnitude, compared to a standard two-color pulse. Boosting the THz yield is confirmed through comprehensive 3D computations that take all propagation effects into account. Selecting the first four Fourier harmonics of the sawtooth waveform already guarantees an impressive increase of the THz energy up to 5 μJ , similar to the record value in [13] but with 100 times smaller total pump pulse energy.

We start with the local current (LC) approximation [17], which neglects propagation effects. The free electron density $\rho(t)$ and current $J(t)$ are governed by

$$\frac{\partial \rho(t)}{\partial t} = W[E(t)] [\rho_0 - \rho(t)], \quad (1)$$

$$\frac{\partial J(t)}{\partial t} = \frac{q^2}{m} \rho(t) E(t) - \frac{J(t)}{\tau_c}, \quad (2)$$

where $E(t)$ is the pump field;

$$W[E(t)] = \frac{\alpha}{|E|} \exp \left[-\frac{\beta}{|E|} \right] \quad (3)$$

is the instantaneous tunnel ionization rate [14], ρ_0 is the density of neutral atoms, q and m are the charge and mass of electron, and τ_c is the current decay time due to collisions. In Eq. (3), $\alpha = 4\omega_a(r_H)^{5/2}E_a$ and $\beta = 2(r_H)^{3/2}E_a/3$ depend on the ratio of the ionization potential U_i of the considered gas over the hydrogen ionization potential, $r_H = U_i/U_H$, while $E_a = m^2q^5/(4\pi\epsilon_0)^3\hbar^4$ and $\omega_a = mq^4/(4\pi\epsilon_0)^2\hbar^3$. The THz field $E_{\text{THz}}(t)$ is generated by the free electrons created by tunnel ionization and then accelerated in the pump field. That is, assuming a small size of the plasma spot, $E_{\text{THz}}(t) \approx g\partial_t J(t)$, where g is a geometrical factor depending on the position of the observer [17].

Ionization mostly happens near the extrema of $E(t)$. In the following, we number their corresponding instants consecutively as $t_1, t_2, t_3, \dots, t_n$. Thus, the electron density and current [Eqs. (1)-(2)] can be approximated as follows (see [17] for details):

$$\rho(t) \simeq \sum_n \delta\rho_n H_n(t - t_n), \quad (4)$$

$$J(t) \simeq J_A(t) + J_B(t), \quad (5)$$

$$J_A(t) = \sum_n q\delta\rho_n v_f(t) H_n(t - t_n), \quad (6)$$

$$J_B(t) = - \sum_n q\delta\rho_n e^{-\frac{t-t_n}{\tau_c}} v_f(t_n) H_n(t - t_n), \quad (7)$$

where $v_f(t)$ is the free electron velocity given by

$$v_f(t) = \frac{q}{m} e^{-\frac{t}{\tau_c}} \int_{-\infty}^t E(t') e^{\frac{t'}{\tau_c}} dt'. \quad (8)$$

The quasi-step function used in Eqs. (4)-(7) is $H_n(t) = \frac{1}{2}[1 + \text{erf}(t/\tau_n)]$, where τ_n is the width of the n th ionization event and the density jump at $t = t_n$, $\delta\rho_n$, is expressed as (see supplemental material)

$$\delta\rho_n \simeq \rho_0 \epsilon_n \left(1 - e^{-\sqrt{\pi}W[E(t_n)]\tau_n}\right), \quad (9)$$

with $\epsilon_1 = 1$ and $\epsilon_n = e^{-\sqrt{\pi}\sum_{j=1}^{n-1} W[E(t_j)]\tau_j}$ for $n > 1$.

Moreover, it is possible to estimate analytically the spectrum of the THz radiation generated by the current components J_A and J_B . We obtain in Fourier space (see supplementary material for a detailed derivation)

$$\mathcal{F}[\partial_t J_B](\omega) \approx \frac{-q}{\sqrt{2\pi}} \sum_n \delta\rho_n v_f(t_n) e^{it_n\omega} \frac{\omega}{i/\tau_c + \omega}, \quad (10a)$$

$$\mathcal{F}[\partial_t J_A](\omega) \approx \frac{-iq^2}{\sqrt{2\pi}m} \sum_n \sum_{k=1}^N \delta\rho_n E_k(t_n) \frac{\omega}{k^2\omega_0^2}. \quad (10b)$$

Here to evaluate $J_A(t)$, we considered multi-color pulses of the form

$$E(t) = \sum_{k=1}^N E_k(t) = \sum_{k=1}^N \mathcal{E}_k(t) a_k \cos(k\omega_0 t + \phi_k), \quad (11)$$

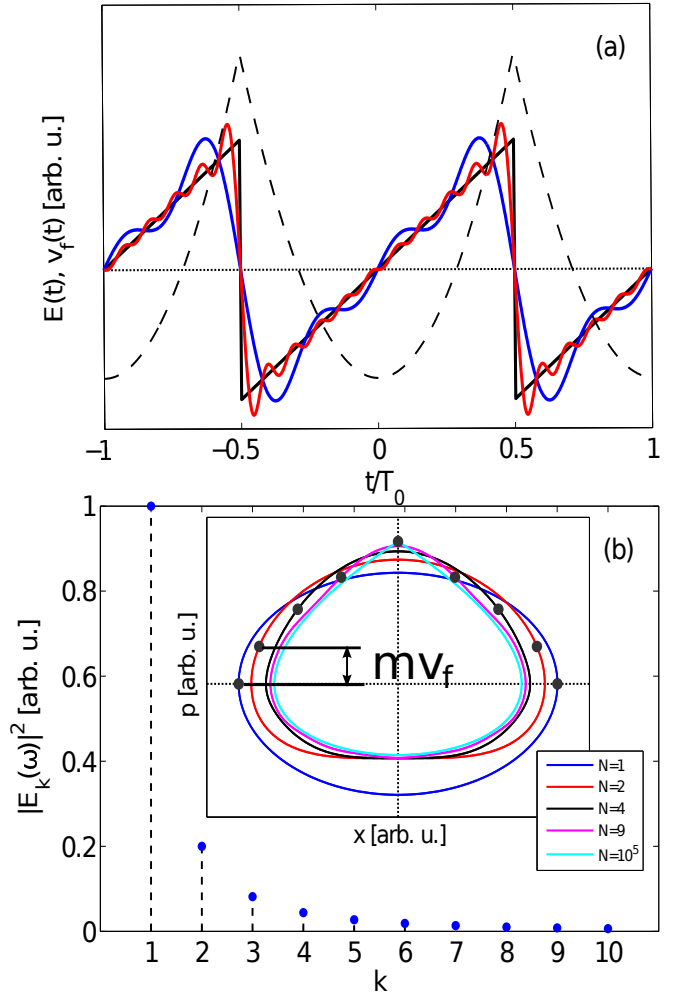


FIG. 1. (a) Sawtooth waveform $E(t)$ (black thick solid line) having the maxima of $v_f(t)$ (black dashed line) at the same instants as the extrema of $E(t)$. Colored solid curves show the three-color (blue curve) and ten-color (red curve) approximations to the ideal sawtooth shape. (b) Spectrum of the sawtooth waveform containing all harmonics of ω_0 with intensities falling down as $1/k^2$. Inset shows the trajectories of free electrons in the phase space (p, x) for an increasing number of colors. Dots locate the maxima of $|E(t)|$; for the 2-color case, the value of mv_f at those maxima is exemplified.

where $\mathcal{E}_k(t)$, a_k and ϕ_k are the envelope with duration τ_k , relative amplitude and phase of the k th harmonic, respectively; ω_0 is the fundamental frequency and we assumed long pulses $\omega_0\tau_k \gg 1$. For a near-infrared pump, the contribution J_B dominates over J_A [22] in the THz spectral range, mainly because the $E_k(t_n)$ are not sign definite and the summands in Eq. (10b) mostly cancel each other. We therefore neglect J_A in the coming analysis. We also assume henceforth Gaussian envelopes $\mathcal{E}_k(t) = E_0 e^{-t^2/\tau^2}$ with amplitude E_0 and duration τ being identical for all colors.

The energy in the THz part of the spectrum below a certain cut-off frequency $\omega_{co} \gg 1/\tau_c$ can be

thus estimated by the local THz yield as $U_{\text{THz}} \propto \int_0^{\omega_{\text{co}}} |\omega \hat{J}_B(\omega)|^2 d\omega \propto \left[\sum_n \delta\rho_n v_f(t_n) \right]^2$. Obviously, to maximize U_{THz} one may not only try to increase the ionization yield $\delta\rho_n$, but also the free electron velocity $v_f(t_n)$. Thus, maximizing the THz energy requires that $v_f(t)$ reaches its extreme values at the discrete instants t_n , and that all $v_f(t_n)$ have the same sign. According to Eq. (8), $v_f(t)$ attains local extrema when $E(t)$ changes its sign. So the only way to achieve maxima of both $|E(t)|$ and $v_f(t)$ at the same instants is to have a discontinuous electric field. This condition is fulfilled by the sawtooth waveform, which can be obtained by setting $a_k = 1/k$ and $\phi_k = (-1)^k \pi/2$ in Eq. (11). The sawtooth waveform and $v_f(t)$ are illustrated by Fig. 1(a) in the limit of negligible free electron collisions, $\tau_c \rightarrow +\infty$. Figure 1(a) also shows that the velocities $v_f(t_n)$ are sign definite.

Practically, as an infinite number of harmonics in the pump is not achievable, we should employ a finite number N of colors. As shown in Fig. 1(a), the sawtooth shape is fairly well reproduced for $N \geq 3$, which is confirmed by the sawtooth spectrum of Fig. 1(b). Inset of this figure details the free electron phase space $p(t) \propto \int_{-\infty}^t E(t') dt' \sim mv_f(t)$ versus $x(t)$, as well as the maximum values of $|E(t)|$ (see dots). One can see that the sign-definite value of $p(t)$ at the field extrema indeed increases with the number of colors, thus increasing U_{THz} .

In the following, we fix ω_0 corresponding to the wavelength $\lambda_0 = 1600$ nm, a choice clearly advantageous over the usual one $\lambda_0 = 800$ nm, because more harmonics are accessible in practice. In particular, the first four harmonics are $\lambda_0/2 = 800$ nm, $\lambda_0/3 = 533$ nm, and $\lambda_0/4 = 400$ nm. All these frequencies can be produced from a 800 nm femtosecond laser source using, for instance, optical parametric amplification to obtain λ_0 and $\lambda_0/3$ and frequency doubling to obtain $\lambda_0/4$. In contrast, for $\lambda_0 = 800$ nm the fourth harmonic at 200 nm lies already in the UV and is not so easy to produce. Throughout the paper, we consider argon at 1 atm pressure and assume a Gaussian pulse envelope with 40 fs FWHM duration ($\tau = 34$ fs).

Let us first check our analytical predictions by computing numerically the local THz yield U_{THz} in the frequency range $\nu \equiv \omega/2\pi < \nu_{\text{co}} \equiv \omega_{\text{co}}/2\pi = 100$ THz from the LC model. For a given multi-color pulse [Eq. (11)] we compute the current $J(t)$ according to Eqs. (1)-(3) and evaluate the local THz yield in Fourier space $U_{\text{THz}} \propto \int_0^{\nu_{\text{co}}} |\nu \hat{J}(\nu)|^2 d\nu$ [23]. From our coming 3D simulations accounting for propagation effects we know that for given pulse energy and focusing conditions the ionization yield for different multi-color configurations is almost the same [see Fig. 3(d)]. This is understandable, because free electrons have a strong defocusing effect and balance the intensity growth in the focal region, similar to the well-

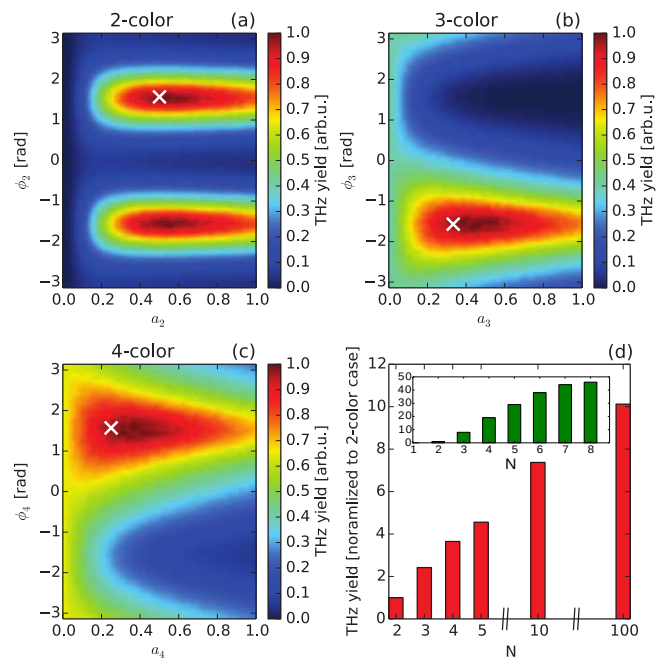


FIG. 2. (a) Dependency of local THz yield on a_2, ϕ_2 for a $N = 2$ color field Eq. (11). (b) Same for a_3, ϕ_3 and $N = 3$. (c) Same for a_4, ϕ_4 and $N = 4$. Relative amplitude and phases of the lower harmonics in (a)-(c) are fixed according to the (optimum) sawtooth shape, i.e., $a_k = 1/k$, $\phi_k = (-1)^k \pi/2$. The total electric field amplitude E_0 is fixed by the ionization yield $\rho^{\text{max}} = 2.7 \times 10^{18} \text{ cm}^{-3}$. White crosses in (a)-(c) indicate the values of the sawtooth waveform. (d) N -color sawtooth THz yield normalized to the 2-color pulse one when ρ^{max} is fixed. For comparison, the inset shows the THz yield for fixed pump energy flux $E_0^2 \sum_k a_k^2$.

known intensity clamping in femtosecond filaments [24]. A reasonable strategy is thus to compare the local THz yield from pulses producing a constant ionization level controlled by $\rho(t \rightarrow +\infty) = \rho^{\text{max}}$ in Eq. (1).

Figure 2 summarizes results from the LC model Eqs. (1)-(3) for Gaussian multi-color pulses with ionization yield ρ^{max} fixed to 10% of ρ_0 . For given a_k and ϕ_k the field amplitude E_0 is chosen such that $\rho^{\text{max}} = 2.7 \times 10^{18} \text{ cm}^{-3}$. First, we fix relative amplitude and phase for the fundamental frequency to $a_1 = 1$, $\phi_1 = -\pi/2$. This choice is arbitrary, because for multi-cycle pulses ($\tau = 34$ fs) carrier-envelope phase effects are negligible. For $N = 4$ colors, we are then left with six free parameters, a_2, a_3, a_4 and ϕ_2, ϕ_3, ϕ_4 . Because we cannot visualize the dependency of the THz yield on all six parameters in the same figure, we treat two-, three-, and four-color cases separately and vary relative amplitude and phase of the highest harmonic only [see Figs. 2(a)-(c)]. Clearly, we observe maximum THz yield for the sawtooth waveform in all cases. We checked that this behavior does not change when one selects the ionization yield to 5% or 50% of ρ_0 .

An interesting issue is how the overall THz signal de-

depends on the number of harmonics that approximates the sawtooth shape. We clarify this question in Fig. 2(d). One can see that the THz yield significantly increases till $N \sim 5$, while its quasi-linear growth saturates for larger N . This behavior is also supported analytically in the supplemental material. There, we also justify that the pump wave shape which optimizes the THz yield approaches the sawtooth one at large N . In the inset of Fig. 2(d) we find it instructive to present the efficiency of the N -color sawtooth approximation in LC limit when the pump energy flux $E_0^2 \sum_k a_k^2$ is fixed, instead of preserving the same ionization level. In this case, the sawtooth shape achieves a more impressive conversion up to a factor of 50 because not only $v_f(t_n)$ but also ρ_n grow considerably. Remarkably, somewhat similar wave shapes were found to increase the yield and electron recollision energy in high-order harmonic generation process by up to two orders of magnitude [25, 26].

The advantage of the four-color approximation of a sawtooth field is now studied using the unidirectional pulse propagation equation that takes into account propagation effects in full space and time resolved geometry. This 3D model was successfully tested against experimental data for THz generation from two-color pulses [27]. We use an adapted version of the unidirectional pulse propagation equation [28] for linearly polarized pulses

$$\partial_z \hat{E} = i \sqrt{k^2(\omega) - k_x^2 - k_y^2} \hat{E} + i \frac{\mu_0 \omega^2}{2k(\omega)} \hat{P}_{\text{NL}}. \quad (12)$$

Here, $\hat{E}(k_x, k_y, z, \omega)$ is the pulse electric field expressed in Fourier domain with respect to transverse coordinates and time, $k = \omega n(\omega)/c$ is the wave number, c is the speed of light and $n(\omega)$ is the linear refractive index of argon [29]. The nonlinear polarization $\hat{P}_{\text{NL}}(\omega) = \hat{P}_{\text{Kerr}}(\omega) + i\hat{J}(\omega)/\omega + i\hat{J}_{\text{loss}}(\omega)/\omega$ accounts for third-order nonlinear polarization $P_{\text{Kerr}}(t)$, electron current $J(t)$ and a loss term $J_{\text{loss}}(t)$ due to photon absorption during ionization. The plasma current $J(t)$ is described by Eqs. (1)-(3). Since 3D propagation affects relative phases, local intensities and pulse durations, we can anticipate a reduced THz conversion efficiency compared with the prediction of Fig. 2(d).

Figure 3(a) displays the pulse spectrum (left axis) and the THz yield below 100 THz (right axis) of a two-color 40-fs pulse with overall energy of $300 \mu\text{J}$. The fundamental wavelength is 800 nm and 6% of the pulse energy is in the second harmonic (SH). The input beam width is $100 \mu\text{m}$, and the pulse is propagating along the longitudinal (z) axis focused over 5-mm focal length in argon at 1 atm pressure. In this classical (non-optimized) two-color setup the THz yield is about $1 \mu\text{J}$. Before passing over to the four-color configuration in Fig. 3(c), let us discuss the second two-color configuration of Fig. 3(b). Here we shift the fundamental wavelength to 1600 nm and augment the SH ratio, which leads to a roughly twofold increase

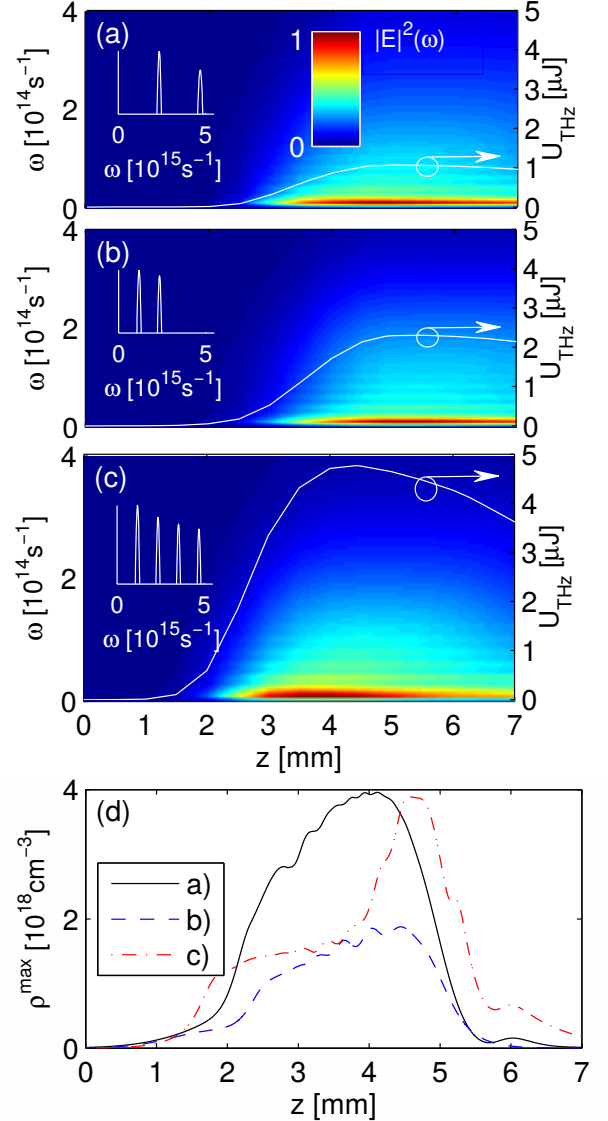


FIG. 3. Low-frequency spectra (image plots) of (a) a two-color pulse for $\lambda_0 = 800$ nm and its second harmonic in respective energy ratio of ≈ 0.06 , (b) a two-color pulse for $\lambda_0 = 1600$ nm and its second harmonic in respective energy ratio of ≈ 0.4 , and (c) a four-color sawtooth pulse for $\lambda_0 = 1600$ nm (thus sum of harmonics energy in ratio ≈ 0.4). The overall THz energy ($\nu < 100$ THz) in the numerical box, $U_{\text{THz}}(z)$, versus z is shown by the right axes. The evolution of the peak free electron density for all three pulses is shown in (d), revealing a comparable fraction ($\approx 10\%$) of the neutral atoms ionized.

of the THz yield. The SH ratio is higher than that prescribed for the sawtooth waveform; however, according to Fig. 2(a) a too large coefficient a_2 has limited impact on the THz yield. It is worth noticing that, by doubling the pump wavelength, only a factor two is achieved in the enhancement of the THz yield. This departs from the order of magnitude increase reported from setups with different focusing conditions in Refs. [19, 30], but remains

consistent with the non-monotonic increase of the THz field strength at high optical intensities ($> 10^{14}$ W/cm²) predicted in [31]. In Fig. 3(c) the results for the four-color configuration are presented with pump pulses up to the fourth harmonic according to the sawtooth waveform. The THz yield is now 5 μ J [see Fig. 3(c)], i.e., 2.5 to 5 times larger than with the two-color cases in Figs. 3(a,b), which agrees with the LC predictions presented in Fig. 2. Finally, the electron density evolution for the three pulses of Figs. 3(a)-(c) is shown in Fig. 3(d). Because pulse energy and focusing conditions are the same, the plasma densities exhibit similar dynamics. In particular, a comparable fraction $\approx 10\%$ of the neutral atoms is ionized in all three cases, justifying the earlier assumption of a constant ionization yield in the local current model.

In conclusion, THz energy depends not only on the number of electrons ionized, but also on the pump field waveform. We have identified the free electron velocity at the time instants of ionization as being crucial for optimizing the THz yield. By exploiting this insight, we have shown that a sawtooth pump shape can boost THz conversion efficiency significantly compared to the standard two-color configuration. Moreover, we provided arguments showing that in the regime of intensity clamping, which unavoidably appears when highest THz energy is targeted, the sawtooth shape is indeed optimal. Comprehensive 3D simulations confirm this finding and reveal

an efficiency of 2%, which is unprecedented for THz generation in gases.

Numerical simulations were performed using high performance computing resources at Rechenzentrum Garching (RZG). AH acknowledges the support of DFG (project HU 1593/2-1). IB is thankful to P. Kinsler for useful discussions.

SUPPLEMENTAL MATERIAL

Expressions of $\rho(t)$, $\frac{d}{dt}J_B(t)$ and $\frac{d}{dt}J_A(t)$

As preliminary computations we introduce the multi-color electric field Eq. (11) into Eq. (3) of the main article, assuming $|E(t)| \ll \beta$. Ionization events occur at the instants t_n of the electric field extrema. In the neighborhood of t_n the absolute value of the electric field is approximated by

$$|E(t)| \approx |E(t_n)| - \frac{1}{2}|\ddot{E}(t_n)|(t - t_n)^2, \quad (13)$$

where $\ddot{E} \equiv \partial_t^2 E$. Following Ref. [17], the ionization rate can be expanded through Taylor series. Using Eq. (13), it is easy to prove by recurrence that odd derivatives of W are approximately zero at $t = t_n$ and even derivatives of W satisfy

$$\frac{d^{2m}}{dt^{2m}}W(|E(t_n)|) \approx (-1)^m (2m - 1)!! W(|E(t_n)|) \left(\frac{\beta|\ddot{E}(t_n)|}{|E(t_n)|^2} \right)^m, \quad m \geq 0, \quad (14)$$

where $p!! = p \cdot (p - 2) \cdot \dots \cdot 3 \cdot 1$ is the double factorial of the odd integer number p [$(-1)!! = 1$].

By substituting Eq. (14) into the Taylor series of the ionization rate, one finds

$$\begin{aligned} \frac{W_n(t)}{W(|E(t_n)|)} &\approx \sum_{m=0}^{\infty} \left[(-1)^m (2m - 1)!! \left(\frac{\beta|\ddot{E}(t_n)|}{|E(t_n)|^2} \right)^m \frac{(t - t_n)^{2m}}{(2m)!} \right] \\ &= \exp \left(-\frac{\beta|\ddot{E}(t_n)|}{2|E(t_n)|^2} (t - t_n)^2 \right), \end{aligned}$$

since $(2m)! = (2m - 1)!! m! 2^m$. The ionization rate around the instant t_n can thus be expressed as

$$W_n(t) \approx W(|E(t_n)|) e^{-\left(\frac{t-t_n}{\tau_n}\right)^2}, \quad (15)$$

where τ_n is interpreted as a characteristic time-length of the ionization event defined by

$$\frac{1}{\tau_n^2} = \frac{\beta|\ddot{E}(t_n)|}{2|E(t_n)|^2} = \frac{1}{3} E_a (U_i/U_H)^{3/2} \frac{|\ddot{E}(t_n)|}{|E(t_n)|^2}. \quad (16)$$

Assuming that the superposition principle holds, we obtain the evaluation of the ionization rate

$$W(t) \approx \sum_n W(|E(t_n)|) e^{-\left(\frac{t-t_n}{\tau_n}\right)^2}. \quad (17)$$

Free electron density

For hydrogen-like atoms, the free electron density is given by Eq. (1) of the paper, yielding

$$\rho(t) = \rho_0 \left[1 - \exp \left(- \int_{-\infty}^t W(\tau) d\tau \right) \right], \quad (18)$$

whenever $\rho(t \rightarrow -\infty) = 0$. Employing Eq. (17) leads to

$$\begin{aligned} \int_{-\infty}^t W(\tau) d\tau &\approx \sum_n \left[W(|E(t_n)|) \int_{-\infty}^t e^{-\left(\frac{t-\tau}{\tau_n}\right)^2} d\tau \right] \\ &= \sum_n \left[\sqrt{\pi} \tau_n W(|E(t_n)|) H_n(t - t_n) \right], \end{aligned} \quad (19)$$

where $H_n(t) = \frac{1}{2}(1 + \text{erf}(t/\tau_n))$ tends to the standard Heaviside step function $\Theta(t)$ when $\tau_n \rightarrow 0$, i.e.,

$$\lim_{\tau_n \rightarrow 0} H_n(t) = \Theta(t) = \begin{cases} 1, & \text{if } t \geq 0, \\ 0, & \text{if } t < 0. \end{cases} \quad (20)$$

To evaluate $\rho(t)$ [Eq. (18)] we exploit the limit given by Eq. (20). First, let us consider a single ionization event. We substitute Eq. (19) for $n = 1$ into Eq. (18) using $H_1(t - t_1) \simeq \Theta(t - t_1)$:

$$\begin{aligned} \rho(t) &= \rho_0 \left(1 - e^{-\sqrt{\pi} \tau_1 W(|E(t_1)|) H_1(t - t_1)} \right) \\ &\approx \rho_0 \left(1 - e^{-\sqrt{\pi} \tau_1 W(|E(t_1)|) \Theta(t - t_1)} \right) \\ &= \rho_0 \left(1 - e^{-\sqrt{\pi} \tau_1 W(|E(t_1)|)} \right) \Theta(t - t_1) \approx \delta \rho_1 H_1(t - t_1), \end{aligned} \quad (21)$$

where $\delta \rho_1$ denotes the density jump of the first ionization event. Second, for two ionization events a similar reasoning yields

$$\begin{aligned} \rho(t) &= \rho_0 \left(1 - e^{-\sqrt{\pi} \tau_1 W(|E(t_1)|) H_1(t - t_1) - \sqrt{\pi} \tau_2 W(|E(t_2)|) H_2(t - t_2)} \right) \\ &\approx \rho_0 \left(1 - e^{-\sqrt{\pi} \tau_1 W(|E(t_1)|) \Theta(t - t_1) - \sqrt{\pi} \tau_2 W(|E(t_2)|) \Theta(t - t_2)} \right) \\ &= \delta \rho_1 \Theta(t - t_1) + \rho_0 \left(1 - e^{-\sqrt{\pi} \tau_1 W(|E(t_1)|) - \sqrt{\pi} \tau_2 W(|E(t_2)|)} - \frac{\delta \rho_1}{\rho_0} \right) \Theta(t - t_2) \\ &\approx \delta \rho_1 H_1(t - t_1) + \delta \rho_2 H_2(t - t_1), \end{aligned} \quad (22)$$

where $\frac{\delta \rho_2}{\rho_0} = \frac{e^{-\sqrt{\pi} \tau_1 W(|E(t_1)|)} - e^{-\sqrt{\pi} \tau_1 W(|E(t_1)|) - \sqrt{\pi} \tau_2 W(|E(t_2)|)}}{e^{-\sqrt{\pi} \tau_1 W(|E(t_1)|)}}$ is the density jump of second ionization event. By a recursive reasoning, we find the following step-wise model for the density

$$\rho(t) = \sum_n \delta \rho_n H_n(t - t_n), \quad (23)$$

where the density jumps for $n > 1$ are defined by

$$\delta \rho_n = \rho_0 e^{-\sum_{j=1}^{n-1} \sqrt{\pi} \tau_j W(|E(t_j)|)} \left(1 - e^{-\sqrt{\pi} \tau_n W(|E(t_n)|)} \right). \quad (24)$$

The free electron density results from the superposition of all step-like ionization events. Equation (24) guarantees that $\rho(t)$ will saturate for high intensities and/or for long laser pulse durations.

THz contribution from $\frac{d}{dt} \mathbf{J}_B(t)$

Following Ref. [17] of the main article, $J(t)$ expresses as

$$J(t) = J_A(t) + J_B(t), \quad (25)$$

$$J_A(t) = q \sum_n [\delta \rho_n v_f(t) H_n(t - t_n)], \quad (26)$$

$$J_B(t) = -q \sum_n \left[\delta \rho_n v_f(t_n) e^{-\frac{t-t_n}{\tau_c}} H_n(t - t_n) \right]. \quad (27)$$

$J_A(t)$ is expected to dominate in the high-frequency part of the spectrum, although for some pulse configurations it may also affect the THz band. In contrast,

the component $J_B(t)$ contributes mostly to low frequencies. According to the LC photo-current model, the field radiated by accelerated electrons is proportional to

$$\mathcal{F}(\partial_t J_B(t)) = -q \sum_n \left[\frac{\delta \rho_n v_f(t_n)}{\sqrt{\pi} \tau_n} \mathcal{F}\left(e^{-\frac{t-t_n}{\tau_c} - \left(\frac{t-t_n}{\tau_n}\right)^2}\right) - \frac{\delta \rho_n v_f(t_n)}{\tau_c} \mathcal{F}\left(e^{-\frac{t-t_n}{\tau_c}} H_n(t-t_n)\right) \right], \quad (28)$$

where, by definition, $\mathcal{F}(f(t)) = \frac{1}{\sqrt{2\pi}} \int_{-\infty}^{+\infty} f(t) e^{i\omega t} dt$.

The first Fourier transform in the right-hand side

$$\mathcal{F}\left(e^{-\frac{t-t_n}{\tau_c} - \left(\frac{t-t_n}{\tau_n}\right)^2}\right) = \frac{\tau_n}{\sqrt{2}} e^{it_n \omega - \frac{1}{4}(\tau_n^2 \omega^2 - \frac{\tau_n^2}{\tau_c^2} + \frac{2i\tau_n^2}{\tau_c} \omega)} \approx \frac{\tau_n}{\sqrt{2}} e^{it_n \omega}, \quad (29)$$

which we approximate in the THz-band ($\omega \rightarrow 0$) using $\omega^2 \ll \omega$ and $\tau_n \ll \tau_c$. THz generation due to this component proceeds from constructive interference of contributions in $e^{it_n \omega}$.

We filter this component in the interval $[0, \omega_{co}]$, where ω_{co} is the cut-off frequency in the THz band, by using the

$$\mathcal{F}\left(e^{-\frac{t-t_n}{\tau_c}} H_n(t-t_n)\right) = \frac{i\tau_c e^{i\omega t_n - \frac{\tau_n^2(i+\tau_c\omega)^2}{4\tau_c^2}}}{\sqrt{2\pi}(i+\tau_c\omega)} \approx \frac{i\tau_c e^{i\omega t_n}}{\sqrt{2\pi}(i+\tau_c\omega)}, \quad (31)$$

which is a peak function lying, in the case of $\omega_{co} \gg 1/\tau_c$, already in the low frequency domain and will thus not be

the derivative of the current. We thus take the time-derivative of Eq. (27) and then apply a Fourier transform, yielding

(RHS) of Eq. (28) is

rectangular filter $\Pi(\omega) = \Theta(\omega + \omega_{co})(1 - \Theta(\omega - \omega_{co}))$, such that

$$\mathcal{F}^{-1}\left(\frac{\tau_n}{\sqrt{2}} e^{it_n \omega} \Pi(\omega)\right) = \frac{\tau_n \omega_{co}}{\sqrt{\pi}} \text{sinc}(\omega_{co}(t-t_n)). \quad (30)$$

The second Fourier transform in the RHS of Eq. (28) expresses as

filtered. Eq. (31), together with Eq. (29) gives Eq. (10a) of the main paper.

The THz component of $\partial_t J_B(t)$ reads as

$$\partial_t J_B^{\text{THz}}(t) = -q \sum_n \left[\delta \rho_n v_f(t_n) \left(\frac{\omega_{co} \text{sinc}(\omega_{co}(t-t_n))}{\pi} - \frac{e^{-\frac{t-t_n}{\tau_c}} H_n(t-t_n)}{\tau_c} \right) \right]. \quad (32)$$

THz contribution from $\frac{d}{dt} \mathbf{J}_A(t)$

Due to the complexity of its expression, we propose an approximate model of $\partial_t J_A^{\text{THz}}(t)$ based on Taylor series and the following approximations:

1. For technical convenience, the slowly-varying envelopes $\mathcal{E}_k(t)$ in Eq. (11) of the main article are

square cosinus with compact support:

$$\mathcal{E}_k(t) \approx E_0 \cos^2\left(\frac{\pi t}{2\tau_k}\right) \Theta(t+\tau_k)(1 - \Theta(t-\tau_k)), \quad (33)$$

where τ_k denotes the duration of the k th color.

2. The pulse has a large number of cycles:

$$\frac{1}{\omega_k} \ll \tau_k. \quad (34)$$

3. We simplify more the free electron density [Eq. (23)] and consider standard Heaviside step functions:

$$\rho(t) = \sum_n \delta\rho_n \Theta(t - t_n). \quad (35)$$

By integrating by parts Eq. (8) of the paper and neglecting time-derivatives of the envelope, we get

$$v_f(t) \approx \frac{q}{m} \sum_{k=1}^N a_k \mathcal{E}_k(t) \frac{\sin(k\omega_0 t + (-1)^k \phi_k)}{k\omega_0}. \quad (36)$$

We take the Fourier transform of Eq. (26) in which we apply Eqs. (35) and (36) with the envelope Eq. (33) to obtain

$$\begin{aligned} \mathcal{F}(J_A(t)) &= q \sum_n \left[\frac{\delta\rho_n}{\sqrt{2\pi}} \int_{-\infty}^{+\infty} v_f(t) H_n(t - t_n) e^{i\omega t} dt \right] \\ &\approx q \sum_n \left[\frac{\delta\rho_n}{\sqrt{2\pi}} \int_{t_n}^{+\infty} v_f(t) e^{i\omega t} dt \right] \\ &\approx \frac{q^2 E_0}{m} \sum_n \sum_k \left[\frac{\delta\rho_n a_k}{\sqrt{2\pi} k \omega_0} \times \right. \\ &\quad \left. \int_{t_n}^{+\infty} \cos^2\left(\frac{\pi t}{2\tau_k}\right) \Theta(t + \tau_k) (1 - \Theta(t - \tau_k)) \times \right. \\ &\quad \left. \sin(k\omega_0 t + (-1)^k \phi_k) e^{i\omega t} dt \right] = \frac{q^2 E_0}{m} \sum_n \sum_k \left[\frac{\delta\rho_n a_k}{\sqrt{2\pi} k \omega_0} \times \right. \\ &\quad \left. \int_{t_n}^{\tau_k} \cos^2\left(\frac{\pi t}{2\tau_k}\right) \sin(k\omega_0 t + (-1)^k \phi_k) e^{i\omega t} dt \right]. \end{aligned}$$

For practical use, we only consider the first two terms in the Taylor expansion of the previous expression around $\omega = 0$. After cumbersome calculations (not detailed), we get

$$\mathcal{F}(\partial_t J_A(t)) = -i\omega \mathcal{F}(J_A(t)) \approx -i\omega \tilde{C}_0 + \omega^2 \tilde{C}_1, \quad (37)$$

$$\tilde{C}_0 = \frac{q^2}{\sqrt{2\pi} m} \sum_n \sum_k \left[\delta\rho_n \frac{E_k(t_n)}{k^2 \omega_0^2} \right], \quad (38)$$

$$\tilde{C}_1 = \frac{q^2}{\sqrt{2\pi} m} \sum_n \sum_k \left[\delta\rho_n t_n \frac{E_k(t_n)}{k^2 \omega_0^2} \right]. \quad (39)$$

This approximation is applicable if the low-frequency range we consider is small compared to ω_0 , that is, $\omega_{co} \ll \omega_0$. Finally, we filter out Eq. (37) using the cut-off frequency ω_{co} to obtain

$$\partial_t J_A^{\text{THz}}(t) \approx C_0 \omega_{co}^2 \text{dsinc}(\omega_{co} t) + C_1 \omega_{co}^3 \text{ddsinc}(\omega_{co} t), \quad (40)$$

$$C_0 = \frac{q^2}{\pi m} \sum_n \sum_k \left[\delta\rho_n \frac{E_k(t_n)}{k^2 \omega_0^2} \right], \quad (41)$$

$$C_1 = -\frac{q^2}{\pi m} \sum_n \sum_k \left[\delta\rho_n t_n \frac{E_k(t_n)}{k^2 \omega_0^2} \right], \quad (42)$$

where $\text{dsinc}(x)$ and $\text{ddsinc}(x)$ denote the first two successive x -derivatives of the function $\text{sinc}(x)$. Equation (10b) of the main paper follows from Eq. (37) and the inequality $|C_1 \omega_{co}^3| \ll |C_0 \omega_{co}^2|$.

Growth of the THz energy with N for fixed ionization degree

The N -color approximation of the sawtooth waveform without envelope is given by

$$E(t) = a_N \sum_{k=1}^N \frac{(-1)^{k+1}}{k} \sin(k\omega_0 t), \quad (43)$$

where a_N is adjusted to the desired ionization degree. The absolute extrema of Eq. (43) are attained at the instants

$$\omega_0 t_n = \pm \frac{N}{N+1} \pi + 2\pi n. \quad (44)$$

After easy manipulations assuming $\tau_c \rightarrow \infty$ for sim-

plicity, the free electron velocity at $t = t_n$ reads as

$$v_f^N(t_n) \propto a_N \chi(N) \equiv a_N \sum_{k=1}^N \frac{(-1)^k}{k^2} \cos\left(\frac{N}{N+1} k\pi\right). \quad (45)$$

Similarly, the value of $E(t_n)$ only depends on the number of color N and so do the maximum ionization rate $W(t_n)$ and the density jumps $\delta\rho_n$. Besides, from Eqs. (28) and (37), one has in Fourier domain

$$\mathcal{F}[\partial_t J](\omega) \approx \frac{-q}{\sqrt{2\pi}} \sum_n \delta\rho_n v_f(t_n) e^{it_n\omega} \frac{\omega}{i/\tau_c + \omega} - i\tilde{C}_0\omega + \tilde{C}_1\omega^2. \quad (46)$$

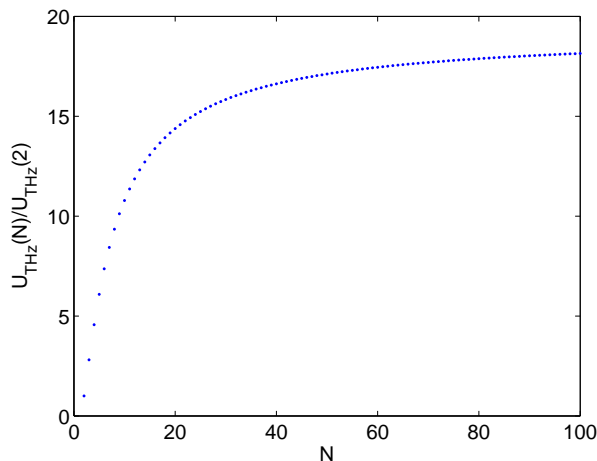


FIG. 4. Growth of the THz energy with the number of harmonics.

For $\omega \gtrsim 1/\tau_c$, every of the first N terms has approximately constant amplitude, whereas the last two terms are $\sim O(\omega)$ and thus typically negligible in THz range.

Thus, to some approximation we can write

$$\mathcal{F}[\partial_t J_{\text{THz}}](\omega) \propto \sum_n \delta\rho_n v_f(t_n) e^{it_n\omega} \equiv B(\omega). \quad (47)$$

Furthermore, $\int_0^{\omega_{co}} BB^* d\omega$ should give the emitted THz energy flux U_{THz} up to a constant factor. For short enough pulses, we assume that the inverse of time intervals $1/(t_n - t_m)$ lies outside the THz range whatever n, m may be, and thus

$$U_{\text{THz}} \propto \left(\sum_n \delta\rho_n v_f(t_n) \right)^2. \quad (48)$$

Accounting for the pulse envelope, U_{THz} is mostly yielded by the contribution, $U_{\text{THz}}(N)$, when Eq. (43) is maximum close to the instants $t = \pm N\pi/[(N+1)\omega_0]$ over the sawtooth period. By taking into account Eq. (45) and the hypothesis of constant ionization level, $\sum_n \delta\rho_n = \text{constant}$, we obtain $U_{\text{THz}}(N) \propto v_f^N(t_n)^2$. To preserve constant ionization, the amplitude a_N must smoothly decrease with the number of colors N . Therefore, using $\chi^2(2) = 9/64$, we can bound from above the growth of the THz energy as

$$\frac{U_{\text{THz}}(N)}{U_{\text{THz}}(2)} \leq \frac{64}{9} \chi^2(N) = \frac{64}{9} \left(\sum_{k=1}^N \frac{(-1)^k}{k^2} \cos\left(\frac{N}{N+1} k\pi\right) \right)^2. \quad (49)$$

Equation (49) is plotted in Fig. 4. Due to the assumptions done, the values are larger than those of Fig. 2(d) in the main paper. Equation (49), however, justifies the saturation in the THz yields reported by the latter figure.

Optimality of sawtooth-like waveforms

In this section we consider another approach to justify the optimality of the sawtooth shape. We consider a sin-

gle cycle of the pump field oscillation and assume a single ionization event there. We optimize $v_f(t_n)$ by varying the wave shape. For technical convenience, we keep both the whole pump intensity and $\delta\rho_n$ constant. We also apply the limit of an infinite decay time $\tau_c \rightarrow +\infty$. The “input” for our optimization procedure is the pump waveform

$$E(t) = E_0 \sum_{k=1}^N a_k \cos(k\omega_0 t + \phi_k), \quad (50)$$

where $\omega_k \equiv k\omega_0$ is the k th harmonic of the fundamental frequency ω_0 . Eq. (50) is obtained from Eq. (11) of the main article assuming constant envelope amplitudes $\mathcal{E}_k(t) \equiv E_0$. Importantly, we consider waveforms having the same average intensity over the pump period:

$$I = \int_{-T_0/2}^{T_0/2} E^2(\tau) d\tau \propto \sum_k a_k^2 = 1. \quad (51)$$

The exact value of the constant on the right hand side is not important, since we optimize the wave shape and not its intensity value. Without loss of generality we assume an extremum of $E(t)$ at $t = 0$ such that

$$\partial_t E(0) = -\sum_k k a_k \omega_0 \sin \phi_k = 0. \quad (52)$$

The quantity to be maximized is then

$$v_f(0) = \frac{q}{m} \sum_k \frac{a_k}{k\omega_0} \sin \phi_k, \quad (53)$$

after choosing the initial time t_0 such that $\sum_k \frac{a_k}{k\omega_0} \sin(k\omega_0 t_0 + \phi_k) = 0$.

It is then evident that, since $v_f(0)$ is linear in $\sin \phi_k$ and assuming all a_k 's having the same sign, the extrema of Eq. (53) are achieved at the phase values $\phi_k = \pm\pi/2$, as expected for the sawtooth phases.

Furthermore, we can rewrite the optimization problem Eq. (53) with constraints Eqs. (51)-(52) in a vectorial form. We introduce the vectors $\mathbf{a} = \{a_1, a_2, \dots, a_N\}$, $\mathbf{b} = \omega_0\{1, 2, \dots, N\}$ and $\mathbf{c} = (1/\omega_0)\{1, 1/2, \dots, 1/N\}$. In the limit of large N , we determine the extremum of (\mathbf{c}, \mathbf{a}) , where (\cdot, \cdot) mean scalar multiplication of two vectors, assuming $(\mathbf{b}, \mathbf{a}) = 0$ and $|\mathbf{a}| = 1$.

The optimum of such a problem is achieved on the vector \mathbf{a} defined by

$$\mathbf{a} = C \left(\mathbf{c} - \mathbf{b} \frac{(\mathbf{b}, \mathbf{c})}{(\mathbf{b}, \mathbf{b})} \right), \quad (54)$$

where the constant C is selected to assure $|\mathbf{a}| = 1$, while $(\mathbf{b}, \mathbf{c}) = N$ and $|\mathbf{b}|^2 \equiv \omega_0^2 S$ with

$$S = \sum_{k=1}^N k^2 = N(N+1)(2N+1)/6. \quad (55)$$

With the previous relations we get

$$a_k = \frac{C}{\omega_0} \left(\frac{1}{k} - \frac{kN}{S} \right). \quad (56)$$

Moreover, one has $|\mathbf{a}|^2 = 1 = C(\mathbf{c}, \mathbf{a})$ and in the limit of large N it is straightforward to obtain

$$C \simeq \frac{(\mathbf{c}, \mathbf{a})\omega_0^2}{\sum_k k^{-2}} \equiv \frac{\omega_0^2}{C \sum_k k^{-2}}, \quad (57)$$

yielding at leading order

$$a_k \simeq \frac{1}{k \sqrt{\sum_{j=1}^N j^{-2}}}, \quad (58)$$

which is the right normalization of the sawtooth amplitude.

For finite N it is easy to show that Eq. (56) approaches the N -truncation of the ideal sawtooth rapidly as N increases. Indeed, from Eq. (56) the deviation in amplitude from the ideal sawtooth profile is yielded by $\delta a_k = -kN/S$, i.e.,

$$|\delta \mathbf{a}|^2 = \frac{N^2}{S^2} \sum_{k=1}^N k^2 = \frac{N^2}{S}. \quad (59)$$

With $S \sim N^3$, $|\delta \mathbf{a}|^2 \sim 1/N$ vanishes as N increases. That is, in this limit, $a_k \rightarrow \text{const}/k$, which means that for large enough number of harmonics the optimal wave shape approaches the sawtooth one.

-
- [1] D. Mittleman, *Sensing with Terahertz Radiation* (Springer, Berlin, 2002).
 - [2] M. Krefß, T. Löffler, M. D. Thomson, R. Dörner, H. Gimpel, K. Zrost, T. Ergler, R. Moshhammer, U. Morgner, J. Ullrich, *et al.*, *Nature Phys.* **2**, 327 (2006).
 - [3] E. Pickwell and V. P. Wallace, *J. Phys. D: Appl. Phys.* **39**, R301 (2006).
 - [4] M. Tonouchi, *Nature Photon.* **1**, 97 (2007).
 - [5] B. Marx, *Laser Focus World* **43**, 44 (2007).
 - [6] W. L. Chan, J. Deibel, and D. M. Mittleman, *Rep. Prog. Phys.* **70**, 1325 (2007).
 - [7] M. C. Hoffmann and J. A. Fülöp, *J. Phys. D: Appl. Phys.* **44**, 083001 (2011).
 - [8] M. Woerner, W. Kuehn, P. Bowlan, K. Reimann, and T. Elsaesser, *New J. Phys.* **15**, 025039 (2013).
 - [9] D. J. Cook and R. M. Hochstrasser, *Opt. Lett.* **25**, 1210 (2000).
 - [10] M. Kress, T. Löffler, S. Eden, M. Thomson, and H. G. Roskos, *Opt. Lett.* **29**, 1120 (2004).
 - [11] T. Bartel, P. Gaal, K. Reimann, M. Woerner, and T. Elsaesser, *Opt. Lett.* **30**, 2805 (2005).
 - [12] K.-Y. Kim, J. H. Glowonia, A. J. Taylor, and G. Rodriguez, *Opt. Express* **15**, 4577 (2007).
 - [13] K. Y. Kim, A. J. Taylor, J. H. Glowonia, and G. Rodriguez, *Nature Photon.* **2**, 605 (2008).
 - [14] H. Roskos, M. Thomson, M. Kress, and T. Löffler, *Laser Photon. & Rev.* **1**, 349 (2007).
 - [15] K. Reimann, *Rep. Prog. Phys.* **70**, 1597 (2007).
 - [16] I. Babushkin, S. Skupin, and J. Herrmann, *Opt. Express* **18**, 9658 (2010).
 - [17] I. Babushkin, S. Skupin, A. Husakou, C. Köhler, E. Cabrera-Granado, L. Bergé, and J. Herrmann, *New J. Phys.* **13**, 123029 (2011).
 - [18] C. Köhler, E. Cabrera-Granado, I. Babushkin, L. Bergé, J. Herrmann, and S. Skupin, *Opt. Lett.* **36**, 3166 (2011).
 - [19] L. Bergé, S. Skupin, C. Köhler, I. Babushkin, and J. Herrmann, *Phys. Rev. Lett.* **110**, 073901 (2013).

- [20] M. Uiberacker *et al.*, *Nature* **446**, 627 (2007).
- [21] A. J. Verhoef, A. V. Mitrofanov, E. E. Serebryannikov, D. V. Kartashov, A. M. Zheltikov, and A. Baltuška, *Phys. Rev. Lett.* **104**, 163904 (2010).
- [22] E. Cabrera-Granado, Y. Chen, I. Babushkin, L. Bergé, and S. Skupin, *ArXiv e-prints* (2014), arXiv:1407.6893.
- [23] Note that here we take into account the total current J , without neglecting J_A .
- [24] L. Bergé, S. Skupin, R. Nuter, J. Kasparian, and J. P. Wolf, *Rep. Prog. Phys.* **70**, 1633 (2007).
- [25] L. Chipperfield, J. Robinson, J. Tisch, and J. Marangos, *Phys. Rev. Lett.* **102**, 063003 (2009).
- [26] S. Haessler, T. Balčiunas, G. Fan, G. Andriukaitis, A. Pugžlys, A. Baltuška, T. Witting, R. Squibb, A. Zair, J. W. G. Tisch, J. P. Marangos, and L. E. Chipperfield, *Phys. Rev. X* **4**, 021028 (2014).
- [27] I. Babushkin, W. Kuehn, C. Koehler, S. Skupin, L. Bergé, K. Reimann, M. Woerner, J. Herrmann, and T. Elsaesser, *Phys. Rev. Lett.* **105**, 053903 (2010).
- [28] M. Kolesik and J. V. Moloney, *Phys. Rev. E* **70**, 036604 (2004).
- [29] A. Dalgarno and A. E. Kingston, *Proc. Royal Soc. London A* **259**, 424 (1960).
- [30] M. Clerici, M. Peccianti, B. E. Schmidt, M. Shalaby, M. Giguère, A. Lotti, A. Couairon, F. Légaré, T. Ozaki, D. Faccio, and R. Morandotti, *Phys. Rev. Lett.* **110**, 253901 (2013).
- [31] A. Debayle, L. Gremillet, L. Bergé, and C. Köhler, *Opt. Express* **22**, 13691 (2014).